frontiers | Frontiers in Environmental Science

TYPE Original Research
PUBLISHED 11 September 2023
DOI 10.3389/fenvs.2023.1098993

OPEN ACCESS

EDITED BY
Jaan H. Pu,
University of Bradford, United Kingdom

REVIEWED BY
Amir Ghaderi,
Urmia University, Iran
Manish Pandey,
National Institute of Technology
Warangal, India

*CORRESPONDENCE
Weijie Wang,
wjwang@whu.edu.cn

RECEIVED 06 January 2023
ACCEPTED 18 April 2023
PUBLISHED 11 September 2023

CITATION
Zhao H, Wang W, Jia F, Wang H, Liu Z and Xu Y (2023), Numerical and analytical flow models in ecological channels with interaction of vegetation and freshwater. *Front. Environ. Sci.* 11:1098993. doi: 10.3389/fenvs.2023.1098993

Numerical and analytical flow models in ecological channels with interaction of vegetation and freshwater

Hanqing Zhao[1,2], Weijie Wang[3]*, Fengcong Jia[4], Huilin Wang[5], Zhiwu Liu[1] and Yuxuan Xu[3,6]

[1]China Three Gorges Corporation, Wuhan, China, [2]National Engineering Research Center of Water Resources Efficient Utilization and Engineering Safety, Nanjing, China, [3]State Key Laboratory of Simulation and Regulation of Water Cycle in River Basin, China Institute of Water Resources and Hydropower Research, Beijing, China, [4]College of Water Resources and Civil Engineering, China Agricultural University, Beijing, China, [5]School of Water Conservancy and Civil Engineering, South China Agricultural University, Guangzhou, China, [6]School of Water Conservancy, North China University of Water Resources and Electric Power, Zhengzhou, China

Aquatic vegetation interferes with river hydrodynamics, thus affecting the mass transport and energy transfer in an ecosystem. The flow over submerged vegetation is characterized by a complex velocity profile and multiple turbulence structures, which have been usually simulated using cylinders or strips in previous studies. Because the simplified vegetation configuration may hide or amplify some physical processes found in natural conditions, we investigate the velocity distribution and turbulence structure in foliaged vegetation flows using both analytical and numerical approaches. The main innovations and findings can be summarized as follows: 1) numerical and analytical models adopted in this paper accurately simulate the flow velocity profile in vegetated channel; 2) the Karman constant is found to be unsuitable for complex vegetation morphologies, so we proposed adjusted coefficient; 3) an image processing method is adopted to quantify the vegetation morphology accurately; 4) the existing mixing-layer thickness formula is found to be unsuitable for vegetation with leaves, an improved formula is proposed showing high correlation coefficient (0.9562) between measured and predicted data; 5) to ensure applicability to larger-scale hydrodynamic simulations, an analytical expression of Manning's coefficient is proposed based on an analytical multi-layer flow velocity model. These research findings can provide theoretical support for the design of vegetated river and ecological restoration.

KEYWORDS

numerical model, analytical model, vegetated flow, velocity profile, Manning's coefficient

1 Introduction

Water flow and associated material, microorganism transport is one of the research hotspots in ecological hydraulics (Wu et al., 2021a; Jiang et al., 2022; Li et al., 2023). The vegetation that is ubiquitous in rivers changes the flow structure, thereby affecting flood conveyance (Katul et al., 2011; Konings et al., 2012), sediment and pollutant transport (Huai et al., 2009; Shucksmith et al., 2010; Huai et al., 2019a; Huai et al., 2019b; Shan et al., 2020; Afzal et al., 2021; Wu et al., 2021b; Zhao and Nepf, 2021), channel evolution (Rominger et al.,

2010; Zhao et al., 2021), and creature activity (Kemp et al., 2000; Bornette and Puijalon, 2011). Ecological channels usually grow a large number of aquatic vegetation. Under the given flow conditions, the velocity distribution characteristics in the river are affected by the vegetation and the shape of the river, and the distribution of vegetation affects the shape of the river. The flow blocking mechanism of vegetation and the turbulent characteristics of flow are related to the river boundary, water level, flow and the type, density and shape of vegetation, and the water quality and ecology along the river were directly improved by vegetation (Huai et al., 2018). Studies on the flow characteristics of ecological channels with vegetation help to clarify the physical and ecological functions of river systems.

Analytical method is the application of analytical formula to solve mathematical models. The analytical model has advantages over the actual laboratory experiment in terms of cost, time and limitations of field collection conditions. Therefore, the further study and improvement of the analytical model has always been the focus of attention of scientists. Owing to the drag exerted by plants, the flow passes over submerged vegetation, the velocity distribution becomes vertically discontinuous and an inflection point occurs at the canopy top (Nepf and Vivoni, 2000). Thus, the profile of the velocity U is S-shaped and no longer follows a logarithmic law (Carollo et al., 2002). Some researchers have simulated vegetated flows numerically by modifying the momentum equation with the canopy drag force formula. For example, Fischer-Antze et al. (2001) solved the three-dimensional Navier–Stokes (3D N-S) equations using the SIMPLE method and the k-ε turbulence model, while Erduran and Kutija (2003) proposed a quasi-3D numerical solution that couples the finite volume solution of the shallow water equations with a finite difference solution of the N-S equations. Zeng and Li (2014) incorporated the Spalart–Allmaras turbulence closure into the 3D N-S model, whereas Pu et al. (2020) combined the improved Shiono-Knight model (SKM) with a Multi-Zonal (MZ) method (proposed by Pu et al., 2020) and applied the proposed analytical model to the flow of rectangular channels. These numerical models can capture the hydrodynamic characteristics of the flow at any point (Lu and Dai, 2016; Yan et al., 2017), Pourshahbaz et al. (2022) compared the numerical model with the experimental results in literature, and found that the overall results of the model better reproduced the measured data,.But their accuracy depends on the parameter settings of the model, which are semi-empirical and suffer from a shortage of suitable guidelines. Other scholars have explored the U profile in an analytical manner by directly solving the N-S equations. This approach represents the kinetic viscosity ν through some turbulence characteristic terms, such as the mixing-length, turbulent kinetic energy, or turbulent kinetic energy dissipation rate (Katul et al., 2004; Poggi et al., 2009; Wang et al., 2018). For example, Katul et al. (2011) found that U exhibits exponential and logarithmic profiles within and above the canopy, respectively; and Cheng et al. (2012) showed that the U profile is exponential above the canopy in a depth-limited flow where the submergence degree is less than 2.

Scientists have not only analyzed the influence of canopy resistance formulas on the U profile of submerged vegetation velocity, but several studies have also explored the profile of U by analyzing motions of turbulent vortices. Vegetated flows are generally characterized by the Kelvin–Helmholtz (KH) vortex, which is driven by the KH instability and billows around the canopy top (Nepf, 2012). Ghisalberti and Nepf (2004) defined the waving region of the KH vortex as the vegetal shear layer (VSL), and observed a hyperbolic tangent profile for U in the exact region. Because the flow below and above the VSL is characterized by wake turbulence and boundary shear turbulence, U is assumed to display constant and logarithmic profiles, respectively (Nezu and Sanjou, 2008). Nikora et al. (2013) proposed a general velocity distribution formula that incorporates multiple turbulent mechanisms to depict the profile of U throughout the water depth. The proposed formula is efficient and accurate, but the VSL boundaries must be provided beforehand. The VSL lower boundary Z_l can be evaluated according to the Reynolds shear stress profile, canopy density, or zero-plane displacement height (Nepf and Vivoni, 2000; Luhar et al., 2008; Nepf and Ghisalberti, 2008). The VSL upper boundary Z_u is assumed to be the critical point at which the U profile deviates downwards from the logarithmic law near the free surface (Nezu and Sanjou, 2008), and can be assessed indirectly by the VSL thickness, which is proportional to the momentum thickness θ. The value of θ is calculated using the flow velocities U_l, U_u at the VSL boundaries and the frequency of the KH vortex f_{KH}, i.e., $\theta = \int_{-\infty}^{+\infty}\{1/4 - [(U - (U_l + U_u)/2)/(U_u - U_l)]^2\} \cdot dz$ or $\theta = 0.016 \cdot (U_l + U_u)/f_{KH}$ (Ho and Huerre, 1984; Ghisalberti and Nepf, 2002). Nepf and Ghisalberti (2008) estimated f_{KH} by analyzing the distribution of the spectral density, which attains its peak at f_{KH}, and showed that f_{KH} is fixed throughout the VSL. In the upper canopy region, where both the KH and wake vortices exist, the spectral distribution is characterized with peaks at both f_{KH} and the wake vortex frequency f_W (Poggi et al., 2004). The spectral density at f_W reflects the coupled actions of both the wake turbulence and the stem scale turbulence (Konings et al., 2012). According to studies on terrestrial canopy flows, the stem scale turbulence is caused by a "spectral shortcut", which interferes with the eddy cascading process by directly breaking up the vegetal shear turbulence (Fathi-Maghadam, 1997). Further studies have shown that the spectral shortcut consumes 58%–71% of the shear turbulent energy, and this action becomes fiercer as the vegetation density increases or the relative submergence decreases (Zhao et al., 2020).

Previous hydrodynamic studies of submerged vegetation have been based on reducing vegetation to cylindrical rods. Finnigan, 2000 pointed out that vegetation cannot be simply considered as a rigid cylinder, because vegetation tends to have complex structural and biomechanical properties, which will produce great deviations in the study of flow resistance and velocity. Recent studies have tended to study vegetated flows with natural-like plant morphologies, because any simplification of the vegetation configuration hides or amplifies some of the physical processes found in natural conditions (Tinoco, 2020). Li et al. (2020) presented the vertical distributions of velocity, Reynolds shear stress, and turbulence intensities in foliaged vegetation flow. Wang et al. (2019) and Zhang et al. (2021) derived analytical solutions for the profile of U in flows over submerged flexible vegetation with variable frontal widths. Tschisgale et al. (2021) explored the interaction between coherent flow structures and vegetation reconfiguration, and discussed the mechanism that drives the wavy motion of the canopy in the Monami regime. Wilson et al. (2003) found that vegetation with foliage increases the canopy drag

force and inhibits vertical momentum exchange, thereby inhibiting the vegetal shear turbulence. Chembolu et al. (2019) showed that a mixed arrangement of different morphologies of vegetation reduces the flow velocity and vegetal shear turbulence, and this shifts the peak Reynolds stress distribution upwards from the canopy top.

In summary, the vegetation morphology affects the motion of the KH and wake vortices and changes the U profile by redistributing the canopy drag (Caroppi and Järvelä, 2022). This study investigates hydrodynamic features such as the turbulence motion and velocity distribution law in an open-channel flow with different types of submerged vegetation. Specifically, we explore the profile velocity using both analytical solutions of the N-S equations and turbulence investigations of the vortex structures, different from existing studies on turbulence structures or analytical solutions of the velocity profile.

2 Theory

2.1 Numerical model

By introducing the resistance term of vegetation into the Reynolds-averaged N-S equations, the momentum equation in the flow direction can be obtained as follows (Luhar et al., 2008; Nepf, 2012):

$$\frac{Du}{Dt} = gS_o - \frac{1}{\rho}\frac{\partial p}{\partial x} - \frac{\partial \overline{u'w'}}{\partial z} + \nu\frac{\partial^2 u}{\partial z^2} - \delta F_d \tag{1}$$

where ν is the kinematic viscosity of water and z is the vertical distance calculated from the bottom of the riverbed.

The critical items in the above equation are

$$K_1 = \frac{\partial \overline{u'w'}}{\partial z} \tag{2}$$

which is the spatially averaged Reynolds stress term,

$$K_2 = \frac{\nu\partial^2 u}{\partial z^2} \tag{3}$$

which is the viscous shear stress, and

$$F_d = \frac{1}{2}C_d m D u^2 \tag{4}$$

which is the vegetation resistance term, i.e., the drag force term. Where $\delta = 1$ in the vegetation layer ($z/h_v < 1$) and $\delta = 0$ above vegetation ($z/h_v > 1$).

Further studies have been carried out for vegetated water flows in the case of a constant uniform flow, and the pressure term expression is as follows:

$$\partial p/\partial x = 0 \tag{5}$$

Subsequently, the flow control equation for constant uniform flow conditions is simplified as

$$gS_o - \frac{\partial \overline{u'w'}}{\partial z} - \delta F_d = 0 \tag{6}$$

For Reynolds stress, the standard K-equation is

$$\overline{u'w'} = -K_m\frac{d\bar{u}}{dz} \tag{7}$$

where K_m is the vortex viscosity coefficient. Substituting the above equation into the control equation gives

$$gS_o + K_m\frac{d^2u}{dz^2} + \frac{dK_m}{dz}\frac{du}{dz} - \frac{\delta}{2}C_d m D u^2 = 0 \tag{8}$$

where C_d is the drag force coefficient. D is water retention width that changes along the vegetation stem, and the variation can be derived in a photography-mathematical method in this article.

To resolve the flow velocity using this equation, the distribution law of the vortex viscosity coefficient needs to be tackled. By means of the Prandtl mixing-length model, we can write

$$K_m = l_{eff}^2\left|\frac{du}{dz}\right| \tag{9}$$

where l_{eff} is the effective mixing-length scale, which is a function of the dominant vortex size.

For the boundary layer on top of the vegetation, the mixing length is

$$l_{eff} = \kappa L_{CBL} = \kappa(z - d) \tag{10}$$

where d is the zero-plane, which can be determined by the following equation:

$$d = \frac{\int_0^{h_v} zF_d(z)dz}{\int_0^{h_v} F_d(z)dz} \tag{11}$$

The vegetation layer contains the entire Karman vortex zone (lower part of the vegetation layer) as well as part of the mixing layer. Under a simplified approach, the mixing length of the vegetation layer can be written as

$$l_{eff} = \psi h_v \tag{12}$$

where ψ is a constant that can be derived from the assumption of continuity of the mixing length over the entire water depth:

$$\psi = \kappa\left(1 - \frac{d}{h_v}\right) \tag{13}$$

2.2 Analytical model

The methods currently used to describe velocity profiles can be divided into three main categories: 1) methods based on the concept of a single profile; 2) methods based on segmented velocity profiles, where the velocity profile is represented by a set of relationships defined for non-overlapping flow zones or segments; and 3) a (linear) superposition based on several traditional concepts applied to the entire flow depth. In contrast to the segment-based model, this paper uses a flow superposition model based on traditional concepts proposed by Nikora et al. (2013), with the innovation that the superposition model is applied to vegetation with a realistic morphology, i.e., the velocity profile can be represented as a superposition of individual profiles formed by specific momentum transport mechanisms. The proposed approach combines these concepts simulatively over the entire

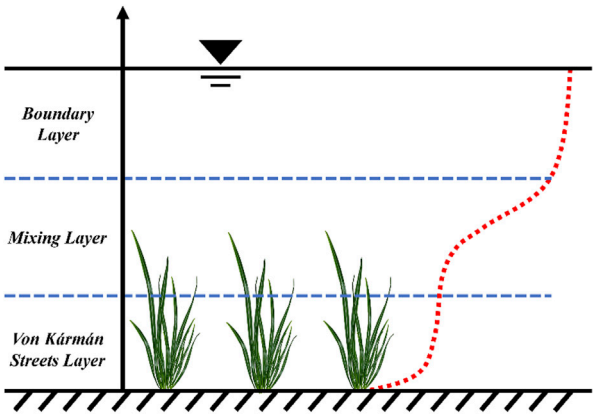

FIGURE 1
Typical diagram of flow velocity distribution in three zones.

flow depth, allowing significant overlaps of momentum transport and turbulence production mechanisms. On this basis, the analysis focuses on the Kármán vortex street zone, the mixing-layer zone, and the boundary layer zone (Figure 1).

2.2.1 Kármán vortex street zone

The vertical variation of the Reynolds stress can be neglected near the bottom, and the vegetation drag force is balanced by the gravity component, so Eq. 6 can be simplified as

$$gS_o - F_d = 0 \tag{14}$$

Furthermore, following Nikora et al. (2013) and Nepf (2012), we can write

$$U_{karman} = \left(\frac{gS_0}{0.5C_d a}\right)^{1/2} \tag{15}$$

where a is the total frontal vegetation area per unit volume, and U_{karman} is flow velocity in the Kármán vortex street zone where the velocity is vertically constant.

2.2.2 Mixing-layer zone

Ei-Hakim and Salama, 1992 argued that Mixing-layer turbulence, formed around the inflectional mean velocity profile which develops between two coflowing streams of different velocities. Ghisalberti and Nepf (2002) implemented this analogy and showed that there is good agreement between velocity profiles measured in their experiments and the hyperbolic tangent law of the mixing layer theory. Nepf and Ghisalberti (2008) proposed two equations to describe the velocity profile gravity. To obtain the complete velocity profile, the submodels proposed for the different layers and zones were combined by imposing various matching conditions (e.g., the velocities and velocity gradients at the boundaries between the different zones should match). Coles (1956) studied the flow velocity distribution by showing that only the logarithmic law occurring in the inner region of the boundary layer is valid and proposed a wake function. Thus, he proposed that the overall velocity profile should be represented "by a linear combination of two universal functions," the law of the wall and the law of the wake. Later, several researchers demonstrated the applicability of this concept to open channel flow [Zhao et al., 2019 and Stoesser et al., 2009].

$$U_{\mathrm{ML}} = U_i + (U_i - U_{\mathrm{Karman}})\tanh\left(\frac{z - z_i}{L_e}\right) \tag{16}$$

where U_i is velocity at the inflection point z_i; and L_e is characteristic length scale of the mixing layer.

2.2.3 Logarithmic rate zone

The logarithmic component of velocity U_{LL} is mainly caused by the proportional variation of turbulence with distance from the bed, and can be represented by the well-known logarithmic law. Kouwen et al. (1969) use the boundary layer concept and the associated logarithmic formula (or logarithmic law) to calculate the velocity distribution above the canopy as

$$\frac{U_{LL}}{u_\star} = \frac{1}{\kappa}\ln\left(\frac{z}{h_v}\right) + C \tag{17}$$

where U_{LL} is the time-averaged velocity, z is the vertical distance from the canopy top, κ is the von Kármán constant, $u_\star$ is the frictional flow velocity, and $C = u_{h_v}/u_\star$.

Ghisalberti and Nepf, 2006 studied the velocity distribution, used the logarithmic section to model, and tried to use the zero plane displacement to move the inflection point. The equation proposed by Kouwen et al. (1969) suffers from the defect that the zero plane, which is the horizontal asymptote of the logarithmic equation, is located at the channel bed. Considering the effect of zero-plane displacement, the logarithmic flow velocity profile of flow above the vegetation should be described as

$$\frac{U_{LL}}{u_\star} = \frac{1}{\kappa}\ln\left(\frac{z - d}{z_o}\right) \tag{18}$$

where z_0 is the hydrodynamic roughness length.

2.3 Turbulent energy spectrum analysis

Spectral analysis of the flow velocity data involves transforming the time domain signal into a frequency domain signal. This enables analysis of the oscillation frequency of the instantaneous flow velocity sequence. The power spectral density is mainly based on the squared value of the flow velocity signal, and the frequency corresponding to the peak power spectral density is the dominant frequency of the vortex. The experimental data are first smoothed and then the power spectral function curve is obtained by applying a Fourier transform to the autocorrelation function of the pulsating flow velocity.

The fast Fourier transform (FFT) is a common method for analyzing the spectral characteristics of turbulent pulsation energy by converting the time-domain flow pulsation signal into a frequency-domain signal. The fluctuating velocity is generally divided into two types: the high frequency and small amplitude fluctuation caused by the small vortex in the turbulence, and the low frequency and large amplitude fluctuation caused by the large vortex. The FFT is applied to the instantaneous flow velocity

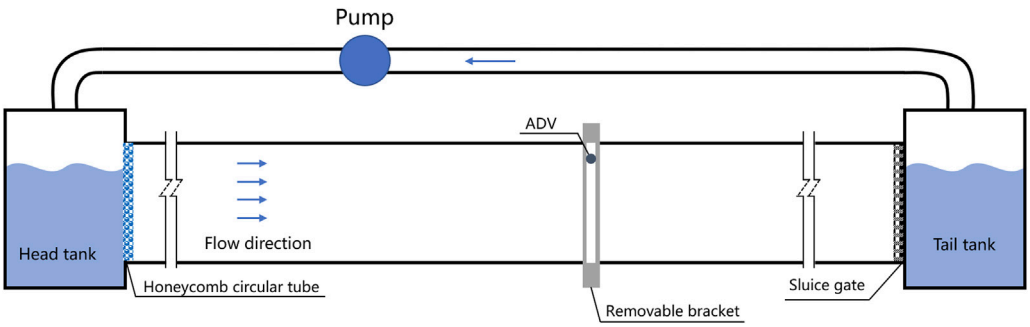

FIGURE 2
Schematic diagram of the submerged vegetation flume test setup.

sequence V, which contains $n = 2^m$ samples. The resulting vector F contains $j = 1\text{-}2^{m-1}$ elements, and satisfies the following equation:

$$F_j = \frac{1}{n}\sum_{k=1}^{n=1} V_k e^{2\pi (j/n)ki} \tag{19}$$

where the amplitude of F is related to the sampling epoch and the number of samples.

3 Experimental setup and program

3.1 Experimental equipment and measurement devices

3.1.1 Experimental equipment

Experiments were completed at the State Key Laboratory of China Institute of Water Resources and Hydropower Research. The experimental set consists of a tank-flume system, simulated vegetation, water ruler, Doppler flow velocity measurement instruments, and related auxiliary facilities. The laboratory has constant heating measures and good ventilation, which ensures stabilities of water temperature and the surrounding environment during the experiment measurement. Figure 2 shows a schematic diagram of the tank-flume system that can be divided into four parts, i.e., an inlet head tank, glass flume, tail tank, and circulation pipe. The glass flume is rectangular and 12 m long, 1 m wide, and 1 m high. A honeycomb structure is installed at the flume entrance to make incoming flow uniform. The flume bed is made of PVC board with magnetic suction bases to locate vegetation elements, and a sluice gate is set at the flume end to maintain the flow depth. The head tank and tail tank is connected by a circulation pipe that is equipped with pump-electromagnetic flowmeter to control the inflow discharge of the flume.

3.1.2 Acoustic Doppler velocity meter

In the experiment, the Acoustic Doppler Velocimeter (ADV) was 200 Hz to measure the velocity field under vegetation flow conditions. The working principle of ADV is based on Doppler Effect, which is mainly composed of signal processing equipment and probe. The probe consists of one transmitter and three receivers. The transmitter generates acoustic waves. If there is a particle movement in the measurement area, the frequency of the acoustic wave reflected by the particles will be different from the original frequency. The three receivers will receive acoustic signals of different frequencies reflected by the particles. The signal processing equipment processes these signals according to the frequency shift principle of Doppler and calculates the instantaneous velocity and movement direction of the particles. The velocity distribution on the whole measuring line is obtained by superimposing the data measured by the probe. The highest sampling frequency is 200 Hz, and the sampling volume is less than 0.09 cm^3. In this experiment, ADV uses a lateral probe, the sampling frequency is 200 Hz, and the sampling time of each point is 120 s. The vertical line spacing is 1cm, and the maximum height measured is 3 cm below the water depth because of the lateral probe. The ADV device is fixed on a customized bracket to ensure the measurement stability during the experiment (Figure 3). The bracket is spatially movable, so the flow velocity at any point can be measured.

3.1.3 Experimental materials

According to the experimental requirements, the vegetation covered bed area of 9 m in length and 1 m in width, and distributed 1 m downstream of the flume inlet. The vegetation type and arrangement were designed to be adjustable. Following research on mudflat areas, the simulated vegetation consisted of dwarf grass with 6 cm height and sedge with 13.5 cm height, and specific parameters of the experimental vegetation are shown in Figure 3.

3.2 Experimental process

3.2.1 Experimental working conditions

To study hydrodynamic characteristics and turbulence development in the rectangular flume, tests were carried out under different vegetation densities and submergence degree conditions. Specific parameters of the tests are listed in Table 1.

3.2.2 Measurement point cross-section

To ensure a relatively complete and in-depth study of the vegetation flow, the onset of turbulence was examined in a preliminary analysis. Turbulent flow was found to be fully developed in the longitude region of x = 400–900 cm.

FIGURE 3
Simulated vegetation experimental area.

TABLE 1 Multi-vegetation pattern test conditions.

Run	Vegetation type	Vegetation height (cm)	Vegetation spacing	Flow depth/cm	Bulk velocity/(cm s^{-1})
1	dwarf grass	6	20 cm × 15 cm (sparse)	30	10
2	dwarf grass	6	20 cm × 15 cm (sparse)	40	7.5
3	dwarf grass	6	10 cm × 7.5 cm (Dense)	30	10
4	Sedge	13.5	20 cm × 15 cm (sparse)	30	10
5	Sedge	13.5	20 cm × 15 cm (sparse)	40	7.5
6	Sedge	13.5	10 cm × 7.5 cm (Dense)	30	10

The measurement points include the vegetated and surrounding areas, and the vegetation was arranged symmetrically along the centerline of the flume. The average values of the flow velocity at $y = 40$ cm and $y = 50$ cm were taken as the plane mean flow velocity for the vegetation spacing of 20 cm × 15 cm; the average values of the flow velocity at $y = 45$ cm and $y = 50$ cm were taken as the plane mean flow velocity for the vegetation spacing of 10 cm × 7.5 cm. The vertical measurement step was set to be 0.05 times the water depth.

3.3 Data processing

When ADV is used to measure turbulent flow, some invalid signals may be collected because of various environmental factors. Therefore, we take some post-processing methods to remove noise signals before calculating velocity values. When removing the interference values from the sample data, four times the standard deviation of the sample was taken as the interval for filtering. The processing method was performed as follows.

First, the overall flow velocity data were processed to remove the interference values in the sample data, i.e., those greater than four times the sample standard deviation. The flow rate sequence obtained with a sampling time of 2 min and sampling frequency of 200 Hz was taken as the data sample, and mean and variance of the data sequence were calculated. When the absolute value of difference between the flow rate signal value $u_i(t)$ and the sample mean was greater than 5 times of the variance, i.e., σ_1, the signal value was considered to be interference, and the two adjacent correct signal values were interpolated to replace the interference signal value.

$$\sigma_1 = \sqrt{\frac{\sum_{i=1}^{N}(u-U)^2}{N}}, \cdots i = 1, 2, 3 \cdots, N \tag{20}$$

where u(t) is the instantaneous velocity in the direction corresponding to the data, U is the time-averaged value of u(t), and N is the total number of samples.

For smaller disturbance values, it is difficult to distinguish them from turbulent pulsations within the flow velocity time series, mainly in the form of large abrupt changes from the preceding and following adjacent flow velocity values. To reflect the nature of continuous variations in the flow velocity, a subtle correction was made to the local abrupt flow velocity data according to the adjacent flow velocity data. The mean and standard deviation of the five flow velocity values before and after the flow velocity at a given point were used to determine whether the flow velocity value at that point was an interference peak.

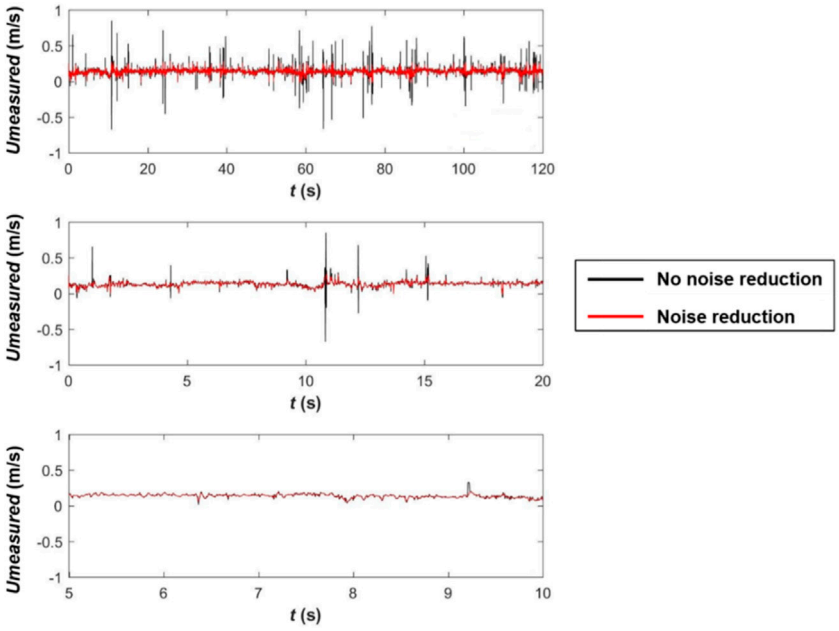

FIGURE 4
Comparison of data before and after noise reduction.

$$\sigma_2 = \sqrt{\frac{\sum_{j=1}^{N}(u - U')^2}{n}}, \cdots i = 1, 2, 3 \cdots, N \tag{21}$$

where $n = 10$ is the number of local data. If the flow velocity at the intermediate point was not within $2\sigma_2$ of the average value, it was regarded as an interference peak.

The noise reduction process effectively removes the interference signal caused by environmental factors, while retaining the true form of the water flow signal. A comparison of the data before and after noise reduction is shown in Figure 4.

4 Results and discussion

4.1 Morphological characteristics of submerged vegetation

In this study, a simulation method was used to measure the diameter of the plant stems. First, the distance between the shooting point and the plant was measured using laser distance measurement technology, and an image of the plant was collected at the shooting point.

$$Gray = 0.299\mathrm{R} + 0.587\mathrm{G} + 0.114\mathrm{B} \tag{22}$$

Where, R represents red pixel, G represents green pixel, and B represents blue pixel. Grayscale image is gray and black and white with different depths, which describes the overall and local chroma and brightness of the image and color image.

The column averages of the recorded data were calculated and divided into a predetermined number of consecutive recognition zones. The demarcation points of the recognition zones were calculated, and the length of the pixel corresponding to the diameter of the plant stem was computed using the pixel coordinates of the two adjacent demarcation points. Finally, the diameter of the plant stem was determined using the length of the pixel, the distance between the shooting point and the plant, and the orientation of the image.

The length of the pixel correspond”ng t’ the diameter of the plant stem is given by

$$L = \sqrt{(\Delta u)^2 + (\Delta v)^2} \tag{23}$$

The plant stem diameter calculation determines the diameter of the plant stem using the following formula:

$$D = L \times S / f \tag{24}$$

This method overcomes the problems of measuring the diameter of plant stems, namely, the low efficiency, poor accuracy, and time-consuming procedure. It also removes the influence of the topography and planting density on the results, and ensures a higher measurement accuracy. Through image processing, the submerged vegetation height h_v corresponding to the two groups of working conditions and the vegetation retaining width D along the vertical variation were obtained. On this basis, the “adaptive” characteristics of vegetation morphology under the water flow environment can be qualitatively determined for dwarf grass and sedge. The vegetation water retention width D along the vertical direction is calculated separately for each working condition. The treatment images are shown in Figure 5A.

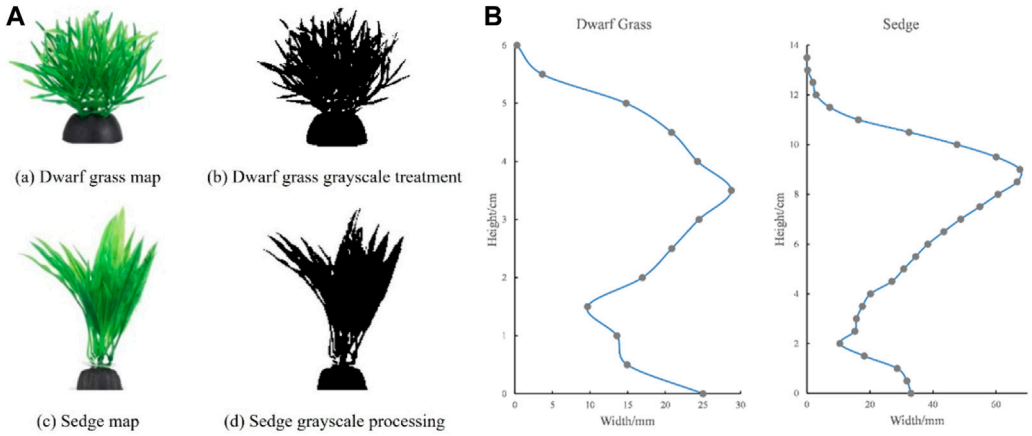

FIGURE 5
(A) Vegetation prototype and grayscale processing; **(B)** Vertical width of underwater morphology of different vegetation.

The underwater morphology of the vegetation and the vegetation water retention width along the vertical direction corresponding to each working condition are shown in Figure 5B. The equivalent widths of the two types of vegetation are found to be 2.73 cm for dwarf grass and 2.97 cm for sedge.

4.2 First-order closure model validation

The results of these spatial analyses of canopy flow are reflected in the traditional vertical profiles of velocity moments. As is readily apparent from a statistical examination of the data, the results are highly dependent on the proximity to the canopy, leading to the generation of very large vertical heterogeneity, especially in vegetated environments with variable vertical orientation. The changes in curvature of the velocity profile, from a logarithmic form in the high-momentum layer above the top of the canopy to an exponential form in the resistance layer below, leads to an inflection point near $z = h_v$. The results indicate that an increase in canopy density leads to enhanced flow characteristics, as shown in Figure 6 for various working conditions, where the flow velocity in the canopy decreases and the shear at the top of the canopy increases. The vertical variation in leaf diameter moderates these effects, which tend to be stronger when more leaves are concentrated in the upper layer. This is especially true in the case of denser vegetation, where the turbulent state in the canopy seems to be mainly determined by the upper canopy elements and is minimally influenced by the lower part of the vegetation.

The specific parameters selected for the numerical calculation of the flow velocity distribution using first-order closure are presented in Table 2. C_d is calculated by adopting method of Cheng and Nguyen (2011):

$$C_d = \frac{130}{r_{v^*}^{0.85}} + 0.8\left[1 - \exp\left(-\frac{r_{v^*}}{400}\right)\right]; r_{v^*} = \left(\frac{gS}{\nu^2}\right)^{1/3}\left(\frac{4 - \pi m D^2}{4mD}\right) \quad (25)$$

As can be seen from Table 2, there is a high correlation between k_v and the vegetation attributes and inundation degree. When the vegetation is relatively short, the value of k_v is large, and when the vegetation height is relatively high, the value of k_v remains basically unchanged. In the environment where the vegetation is short, an increase in the inundation degree enhances the value of k_v, which explains why the vegetation height produces a difference in diameters. Specific simulation results are shown in Figure 6.

4.3 Flow rate superposition model validation

4.3.1 Turbulent energy spectrum analysis

This subsection investigates the turbulent structure of the shear layer formed at the interface between the vegetated and non-vegetated zones. The KH instability leads to the formation of vortex structures within the shear layer. These vortex structures dominate the lateral transport of energy as well as momentum, which is reflected at the interfacial interface, where periodic fluctuations in velocity and Reynolds stress occur. The longitudinal and transverse flow velocities are inversely correlated, indicating that there is a strong momentum exchange at the intersection, and the strong sweep is accompanied by weak promotion. The approximate periodicity of velocity and Reynolds stress proves that there is a dominant frequency of the vortex structures at the intersection, and energy spectrum density analysis can be used to determine this dominant frequency.

The vegetation morphology affects the vortices generated by the water flow when passing through the submerged vegetation. In general, the turbulence intensity of the water flow increases with increasing flow velocity, whereupon the vortex propagation frequency becomes faster. Therefore, the flow velocity sequence on top of the vegetation is analyzed using the energy spectrum, and then the propagation frequency and energy dissipation law of turbulence are determined.

Spectrum analysis indicates that, under the influence of the vegetation properties and the distribution method, the water flow produces large and small vortices near the lower edge of the vegetation cover. These vortices cause strong periodic oscillations and momentum transport in the flow, specifically the periodic oscillation of the longitudinal flow velocity and vertical Reynolds

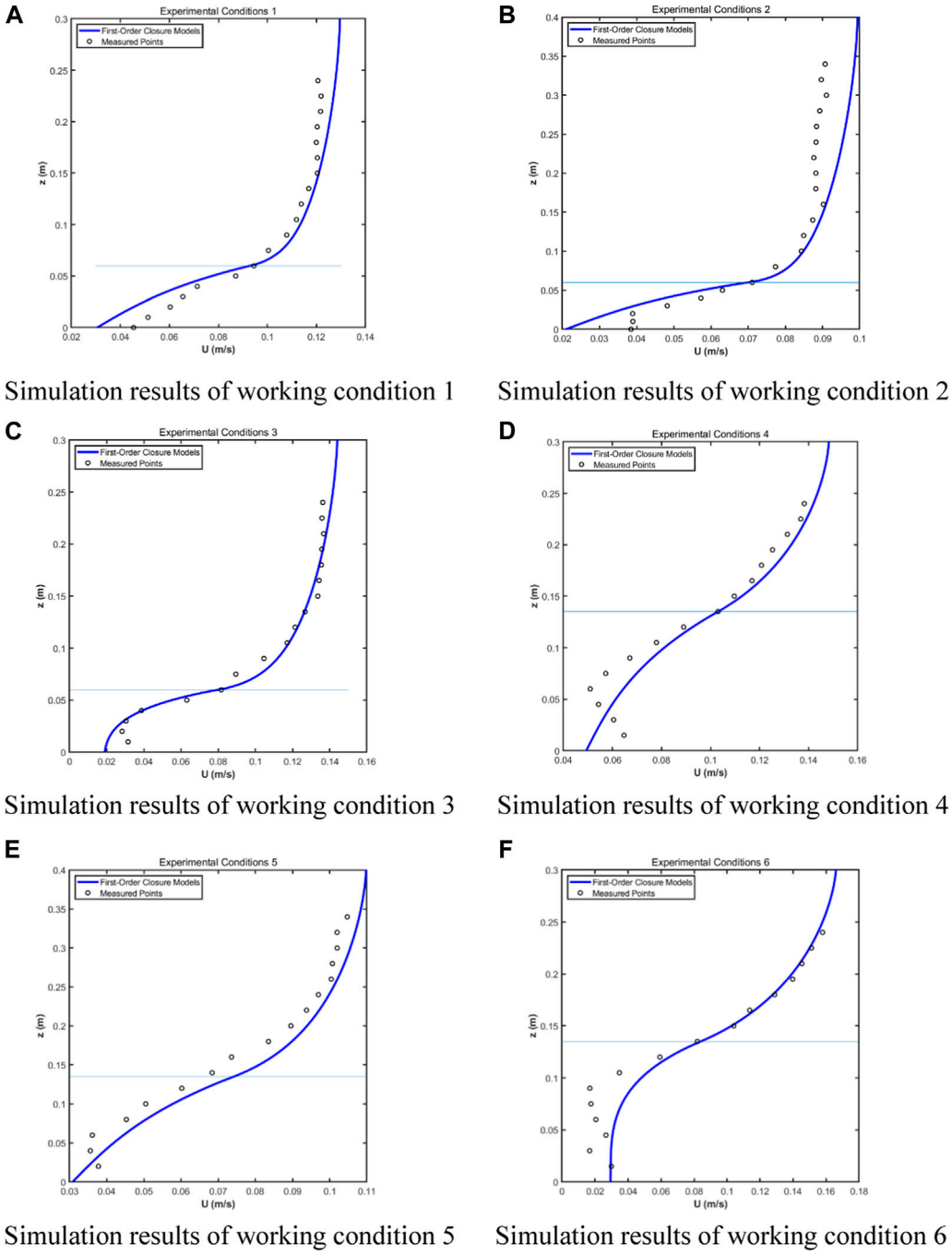

FIGURE 6
Simulation of the first-order closed model for working condition 1–6 **(A–F)**.

stress. Analysis of the peak frequency of the energy spectrum (Figure 7) shows that the distribution of the energy spectrum satisfies the −5/3 power law.

Further analysis of the water flow in the fully developed region (x/l_{veg} = 0.61) indicates that the dominant frequency of the eddies varies considerably at the vegetation intersections. The dimensionless Strouhal number (S_t) describes the relationship between the frequency of eddy shedding and the characteristic length of the obstacle, and is widely used in conditions where the Karman vortex street or the stem turbulence generating term P_w is dominant. S_t is calculated as

$$S_t = \frac{fL}{U} \tag{26}$$

where f is the vortex frequency, i.e., the dominant frequency in the energy spectrum analysis, L is the characteristic length of the vortex size, and U is the characteristic flow velocity (usually the traveling flow velocity near the obstacle). For a large range of Reynolds

TABLE 2 First-order closure model parameters.

Conditions	h_w (m)	h_v (m)	m (Stem/m^2)	S	k_v	D (m)	C_d	RMSE	R
1	0.3	0.06	33.3	0.0001	1.81	0.052	1.2146	0.007645784	0.9968
2	0.4	0.06	33.3	0.00005	2.3	0.052	1.2836	0.007438259	0.9942
3	0.3	0.06	133.3	0.00019	1.3	0.042	1.8689	0.005133355	0.994
4	0.3	0.135	33.3	0.00015	0.41	0.033	1.1001	0.007070949	0.9821
5	0.4	0.135	33.3	0.000045	0.59	0.025	1.1166	0.005625299	0.9929
6	0.3	0.135	133.3	0.0004	0.41	0.042	1.629	0.010235187	0.9935

numbers, Huai et al., 2021 noted that $S_t = 0.21$. Poggi et al. (2004) found that *St* tends to remain constant as the rigid vegetation density varies.

Using Nepf's formula, which differs significantly from our measured values, we have

$$f_{\mathrm{KH}} = 0.032\left(\frac{\bar{U}}{\theta}\right) \tag{27}$$

whereas Ho et al. (1991) suggested that

$$\theta = \int_{-\infty}^{\infty}\left[\frac{1}{4} - \left(\frac{U-\bar{U}}{\Delta U}\right)^2\right]dz \tag{28}$$

The presence of vegetation strongly changes the cross-sectional distribution of mean streamwise velocity. This parameter is obtained by separating the average velocity and instantaneous velocity fluctuation of each velocity component (Hopkinson and Wynn, 2009). Compared with non-vegetated flow, the change of vegetation-driven turbulence is a function of physical parameters such as vegetation type (flexibility and rigidity), relative submergence (submergence and outflow) and density (sparse and dense). In the case of complete submergence, the vegetation changes the velocity and turbulence intensity profiles, forming a vertical mixing layer near the top of the S-shaped velocity profile at the inflection point (Ghisalberti and Nepf, 2002). This mixing layer is a large-scale coherent vortex with properties, which convections the high momentum fluid to the low momentum fluid region in the canopy. This mechanism can be further modified. The energy spectrum density analysis method is used to process the interface velocity, and the peak energy spectrum density corresponds to the dominant frequency of the continuous vortex structure.

4.3.2 Flow rate superposition model

Most studies on the hydrodynamic characteristics of aquatic plant canopies under inundation have recognized that their time-averaged flow velocity distributions have inflection points near top of the canopy. Several studies have also recognized hyperbolic-type distributions. Shi et al., 2023 derived hyperbolic sine and hyperbolic cosine distribution patterns above the canopy through an analytical approach. By adjusting each parameter in them, these functional expressions were able to obtain better agreement with the measured values. Researchers believe that the logarithmic distribution of the time-averaged flow velocity is the result of turbulent motion in the boundary layer, while the inverse tangent or hyperbolic distribution with an inflection point is the result of turbulent vertical mixing in the mixed layer. The essence of the former is the submerged aquatic plant canopy forming a rough boundary layer in the flow. The boundary layer above the canopy turbulent vortices does not penetrate the interior of the canopy, and is thus unaffected by the mixing of the two layers of water inside and outside the canopy. The essence of the latter is the plant canopy providing a rough pore medium for water flow through the canopy, whereby the two layers of different velocities inside and outside the canopy mix with each other to produce mixed-layer turbulent vortices, thus causing momentum exchange in the upper region. Nikora et al. (2013) derived a third type of distribution, namely, segmental superposition, which replicates the characteristics of interconnectedness and smoothness between the segments by superposition. A flow velocity superposition diagram is shown in Figure 8.

The analytical model was applied to solve the model using the parameters presented in Table 3.

For experimental conditions including flexible vegetation, a genetic algorithm gives

$$f_{\mathrm{KH}} = 0.113\left(\frac{\bar{U}}{\theta}\right) \tag{29}$$

Compared with Eq. 30, Nepf formula and Eq. 30 were used to calculate f_{KH}. The correlation coefficient of Nepf formula was −0.5015, and that of Eq. 30 was 0.9562, indicating a great improvement in simulation accuracy (see Figure 9).

4.4 Manning's coefficient: Theoretical formula to solution

Manning's formula is used to calculate the resistance coefficient of water flow in rivers and wetlands, such as in river flow calculations, flood control analysis, and watershed water transfer. The complexity of actual river flow states requires extended and modified versions of Manning's formula. However, the specific expression of Manning's formula for vegetated rivers under nonuniform hook flow conditions remains unclear. As the core parameter in Manning's formula, this paper presents an equation for calculating Manning's coefficient for vegetated rivers. Using

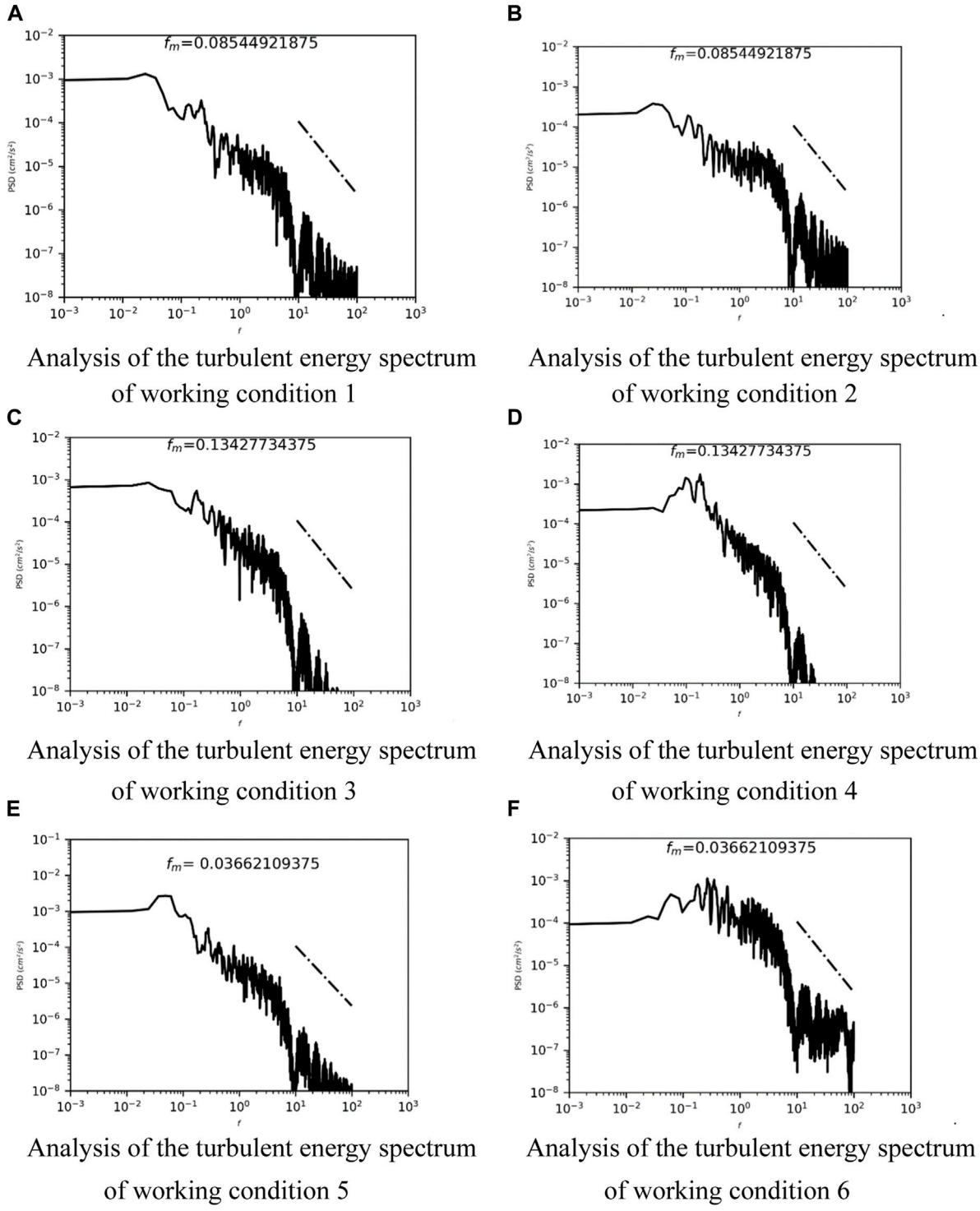

FIGURE 7
Analysis of turbulent energy spectrum for working condition 1–6 **(A–F)**.

this coefficient, we can then derive Manning's formula in nonuniform flow conditions. Manning's coefficient can be expressed as

$$U = \frac{1}{n} R^{2/3} S^{1/2} \tag{30}$$

The analytical solution for the flow velocity is averaged in the water depth direction to obtain the section average flow velocity, which is substituted into Eq. 30 to obtain the Manning's coefficient equation for the reference flow velocity superposition model. The linear superposition model equation can be expressed as

10.3389/fenvs.2023.1098993

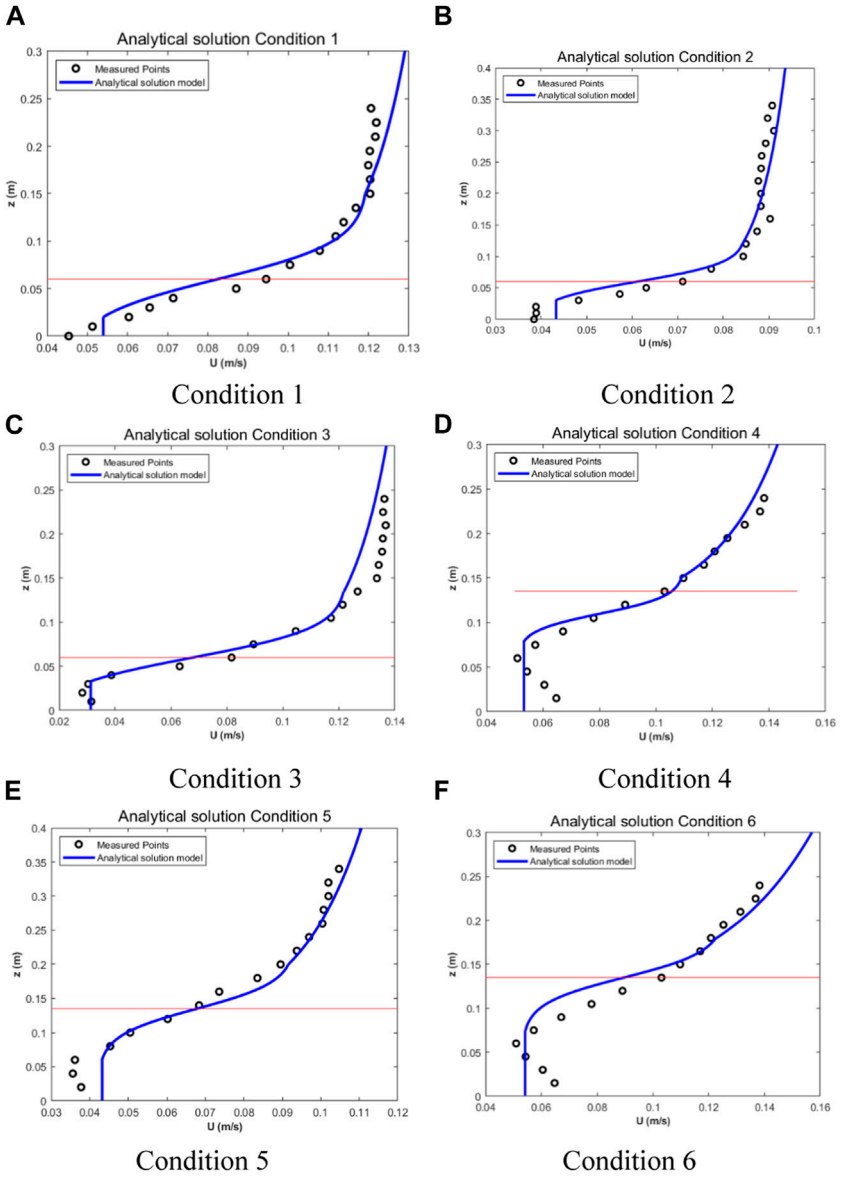

FIGURE 8
Analytical solutions of the flow velocity distribution for working condition 1–6 **(A–F)**.

TABLE 3 Parameters of superposition model.

Run	Shear vortex frequency (Hz)	U_1 (m/s)	U_2 (m/s)	d (m)	Z_0 (m)	θ (m)	*RMSE*	*R*
1	0.085449219	0.12	0.045	0.048	0.00000175	0.020	0.005774345	0.9801
2	0.085449219	0.085	0.0375	0.048	0.0000000495	0.015	0.004464172	0.9745
3	0.134277344	0.123	0.0125	0.048	0.000017	0.017	0.006171732	0.994
4	0.134277344	0.11	0.0507	0.108	0.000345	0.01	0.004990359	0.9918
5	0.036621094	0.0935	0.042	0.108	0.00035	0.02	0.003981397	0.9934
6	0.036621094	0.126	0.053	0.108	0.002118	0.015	0.008239536	0.9821

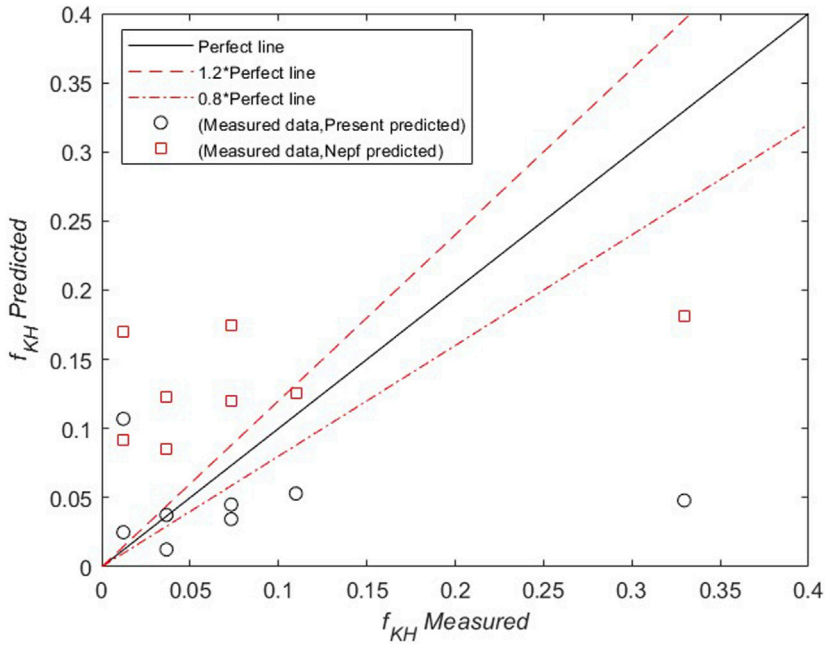

FIGURE 9
Comparison of measurements with f_{KH} of Nepf (2012) and predicted f_{KH} of present study.

$$\frac{U_f}{u_{*b}} = \underbrace{\frac{1}{u_{*b}}\left(\frac{gS_b}{0.5C_D a}\right)^{1/2}}_{\text{Unifrom Distribution}} + \underbrace{\frac{(U_i - U_{karman})}{u_{*b}}\left[1 + \tanh\left(\frac{z - z_i}{L_e}\right)\right]}_{\text{Mixing Layer}} \times \underbrace{+\frac{u_{*m}}{u_{*b}}\frac{1}{\kappa}\ln\left(\frac{z - z_i - d_i}{z_o}\right)}_{\text{Log Layer}} \tag{31}$$

The expression for Manning's coefficient can be solved by performing a segmental integration of the following terms.

(1) U_{karman}

$$U_1 = \frac{1}{Z_1}\int_0^{Z_1} U_{karman} dZ = \left(\frac{gS_b}{0.5C_d a}\right)^{1/2} \tag{32}$$

Where 0~Z_1 is the zone of Karman vortex.

(2) U_{ML}

$$U_2 = \frac{1}{Z_2 - Z_1}\int_{Z1}^{Z2} U_{ML} dZ = \frac{\left\{\bar{u} + \frac{\Delta u \cdot m}{2}\cdot \ln\left[\cosh\left(\frac{z-\bar{z}}{Lm}\right)\right]\right\}\Big|_{z=z_2} - \left\{\bar{u} + \frac{\Delta u \cdot Lm}{2}\ln\left[\cosh\left(\frac{z-\bar{z}}{\mathrm{Lm}}\right)\right]\right\} \mid z = z_1}{Z_2 - Z_1} \tag{33}$$

Where Z_1~Z_2 is the zone of Mixing layer.

(3) U_{LL}

$$U_3 = \frac{1}{h_w - Z_2}\int_{Z_2}^{h_w} U_{ML} dZ = \frac{1}{h_w - Z_2}\left\{\frac{u_*}{k}\left[-Z + (Z-d)\ln\left(\frac{Z-d}{Z_0}\right)\right]\Big|_{Z=h_w} - \frac{u_*}{k}\left[-Z + (Z-d)\ln\left(\frac{Z-d}{Z_0}\right)\right]\Big|_{Z=Z_2}\right\} \tag{34}$$

Where Z_2~h_w is the Logarithmic rate region.

The resistance of water flow in a river channel directly affects the water level and water distribution in the basin. Simulations of the hydraulic process in a river channel using a mathematical model require the relevant resistance characteristics. The resistance of a vegetated river channel under nonuniform flow conditions mainly consists of two parts: the resistance caused by the rough form of the river itself and the resistance caused by the vegetation blocking water. The presence of vegetation causes the water depth and flow velocity to vary along the course, forming a constant nonuniform flow. In this case, we must consider both along-range energy loss and local resistance energy loss, which leads to the calculation formula for Manning's coefficient.

$$U_b = \frac{U_1 Z_1 + U_2 (Z_2 - Z_1) + U_3 (h_w - Z_2)}{h_w} \tag{35}$$

Combining Eqs. 30, 35, we obtain

$$n = R^{2/3} S^{1/2} \Big/ \times \left\{ \begin{array}{c} Z_1^{\,2}\left(\frac{gS_b}{0.5C_D a}\right)^{1/2} + \left\{\bar{u} + \frac{\Delta u \cdot m}{2}\cdot \ln\left[\cosh\left(\frac{z_2 - \bar{z}}{L_m}\right)\right]\right\} \\ -\left\{\bar{u} + \frac{\Delta u \cdot Lm}{2}\ln\left[\cosh\left(\frac{z_1 - \bar{z}}{L_m}\right)\right]\right\} + \left[\left(\frac{-u_* d}{k}\ln\left(\frac{h_w - d}{Z_0}\right) + \frac{u_* d}{k}\ln\left(\frac{Z_2 - d}{Z_0}\right)\right)\left(\frac{h_w - Z_2}{h_w}\right)\right] \end{array} \right\} \tag{36}$$

5 Conclusion

The first-order closure model and analytical models were used to calculate and analyze the flow velocity distribution in a vegetated rectangular channel. Using experimental data from actual measurements and correlation coefficients gives results that are in good agreement with the actual measurements. This confirms that the application of both models to vegetated river channels is feasible.

The conclusions from this study can be summarized as follows: 1) Both the numerical model and the analytical model proposed in this paper can accurately simulate the water flow movement under the influence of vegetation. 2) In scenarios where Karman's constant is not applicable to complex vegetation morphologies, we have proposed a new Karman coefficient. 3) We adopted an image processing method to quantify the vegetation morphology accurately. 4) As the existing mixed-layer thickness formula is not applicable to vegetation with leaves, we have derived an improved approach. 5) To ensure applicability to larger-scale hydrodynamic simulations, we proposed an expression for Manning's coefficient based on the multi-layer flow velocity analytical solution model. Finally, we demonstrated the variation characteristics of Manning's coefficient with respect to the inundation degree, which provides theoretical support for vegetated river design and ecological restoration.

Data availability statement

The original contributions presented in the study are included in the article/supplementary material, further inquiries can be directed to the corresponding author.

Author contributions

Conceptualization: WW and HZ, methodology: WW and HZ, data analysis and modelling: WW, FJ, HW, and ZL, writing-original draft: FJ, HZ, and WW, writing-review and editing: WW, HZ, and YX. All authors contributed to the article and approved the submitted version.

Funding

This work was financially supported by a Scientific Research Project of the China Three Gorges Corporation (202103399), and Talent Program of China Institute of Water Resources and Hydropower Research (WE0199A052021), National Natural Science Foundation of China (52209083, 51809286).

Conflict of interest

HZ and ZL were employed by China Three Gorges Corporation.

The remaining authors declare that the research was conducted in the absence of any commercial or financial relationships that could be construed as a potential conflict of interest.

Publisher's note

References

Afzal, M. S., Holmedal, L. E., and Myrhaug, D. (2021). Sediment transport in combined wave–current seabed boundary layers due to streaming. *J. Hydraulic Eng.* 147 (4), 04021007. doi:10.1061/(asce)hy.1943-7900.0001862

Bornette, G., and Puijalon, S. (2011). Response of aquatic plants to abiotic factors: A review. *Aquat. Sci.* 73, 1–14. doi:10.1007/s00027-010-0162-7

Carollo, F. G., Ferro, V., and Termini, D. (2002). Flow velocity measurements in vegetated channels. *J. Hydraulic Eng.* 128 (7), 664–673. doi:10.1061/(asce)0733-9429(2002)128:7(664)

Caroppi, G., and Järvelä, J. (2022). Shear layer over floodplain vegetation with a view on bending and streamlining effects. *Environ. Fluid Mech.* 22, 587–618.

Chembolu, V., Kakati, R., and Dutta, S. (2019). A laboratory study of flow characteristics in natural heterogeneous vegetation patches under submerged conditions. *Adv. Water Resour.* 133, 103418. doi:10.1016/j.advwatres.2019.103418

Cheng, N. S., and Nguyen, H. T. (2011). Hydraulic radius for evaluating resistance induced by simulated emergent vegetation in open-channel flows. *J. hydraulic Eng.* 137 (9), 995–1004. doi:10.1061/(asce)hy.1943-7900.0000377

Cheng, N. S., Nguyen, H. T., Tan, S. K., and Shao, S. (2012). Scaling of velocity profiles for depth-limited open channel flows over simulated rigid vegetation. *J. Hydraulic Eng.* 138 (8), 673–683. doi:10.1061/(asce)hy.1943-7900.0000562

Ei-Hakim, O., and Salama, M. M. (1992). Velocity distribution inside and above branched flexible roughness. *J. Irrigation Drainage Eng.* 118 (6), 914–927. doi:10.1061/(asce)0733-9437(1992)118:6(914)

Erduran, K. S., and Kutija, V. (2003). Quasi-three- dimensional numerical model for flow through flexible, rigid, submerged and non-submerged vegetation. *J. Hydroinformatics* 5, 189–202. doi:10.2166/hydro.2003.0015

Fathi-Maghadam, M. N Kouwen. Nonrigid nonsubmerged Vegetative roughness on floodplains.*Jounral Hydraulic Eng.*, 1997,1 23(1):51–57.

Finnigan, J. Turbulence in plant canopies. *Annu. Rev. Fluid Mech.*, 2000, 32: 519–571.

Fischer- Antze, T., Stoesser, T., Bates, P., and Olsen, N. (2001). 3D numerical modelling of open-channel flow with submerged vegetation. *J. Hydraulic Res.* 39 (3), 303–310. doi:10.1080/00221680109499833

Ghisalberti, M., and Nepf, H. M. (2002). Mixing layers and coherent structures in vegetated aquatic flows. *J. Geophys. Res.* 107 (C2), 3011. doi:10.1029/2001jc000871

Ghisalberti, M., and Nepf, H. M. (2004). The limited growth of vegetated shear layers. *Water Resour. Res.* 40, W07502. doi:10.1029/2003wr002776

Ghisalberti, M., and Nepf, H. M. (2006). The structure of the shear layer in flows over rigid and flexible canopies. *Environ. Fluid Mech.* 6, 277–301. doi:10.1007/s10652-006-0002-4

Ho, C. M., and Huerre, P. (1984). Perturbed free shear layers. *Annu. Rev. Fluid Mech.* 16, 365–422. doi:10.1146/annurev.fl.16.010184.002053

Hopkinson, L., and Wynn, T. (2009). Vegetation impacts on near bank flow[J]. Ecohydrology: Ecosystems, land and water process interactions. *Ecohydrogeomorphology* 2 (4), 404–418. doi:10.1002/eco.87

Huai, W. X., Shi, H. R., Song, S. W., and Ni, S. (2018). A simplified method for estimating the longitudinal dispersion coefficient in ecological channels with vegetation. *Ecol. Indic.* 92, 91–98. doi:10.1016/j.ecolind.2017.05.015

Huai, W. X., Li, S., Katul, G. G., Liu, M. y., and Yang, Z. h. (2021). Flow dynamics and sediment transport in vegetated rivers: A review. *J. Hydrodynamics* 33 (3), 400–420. doi:10.1007/s42241-021-0043-7

Huai, W. X., Yang, L., Wang, W. J., Guo, Y. K., Wang, T., and Cheng, Y. G. (2019a). Predicting the vertical low suspended sediment concentration in vegetated flow using a random displacement model. *J. Hydrology* 578, 124101. doi:10.1016/j.jhydrol.2019.124101

Huai, W. X., Zeng, Y. H., Xu, Z. G., and Yang, Z. (2009). Three-layer model for vertical velocity distribution in open channel flow with submerged rigid vegetation. *Adv. Water Resour.* 32, 487–492. doi:10.1016/j.advwatres.2008.11.014

Huai, W. X., Zhang, J., Katul, G. G., Cheng, Y. g., Tang, X., and Wang, W. j. (2019b). The structure of turbulent flow through submerged flexible vegetation. *J. Hydrodynamics* 31 (2), 274–292. doi:10.1007/s42241-019-0023-3

Jiang, W., Zeng, L., Fu, X., and Wu, Z. (2022). Analytical solutions for reactive shear dispersion with boundary adsorption and desorption. *J. Fluid Mech.* 947, A37. doi:10.1017/jfm.2022.656

Katul, G. G., Mahrt, L., Poggi, D., and Sanz, C. (2004). One- and two-equation models for canopy turbulence. *Boundary- Layer. Meteorol.* 113, 81–109. doi:10.1023/b:boun.0000037333.48760.e5

Katul, G. G., Poggi, D., and Ridolfi, L. (2011). A flow resistance model for assessing the impact of vegetation on flood routing mechanics. *Water Resour. Res.* 47 (8), W08533. doi:10.1029/2010wr010278

Kemp, J. L., Harper, D. M., and Crosa, G. A. (2000). The habitat-scale ecohydraulics of rivers. *Ecol. Eng.* 16, 17–29. doi:10.1016/s0925-8574(00)00073-2

Konings, A. G., Katul, G. G., and Thompson, S. E. (2012). A phenomenological model for the flow resistance over submerged vegetation. *Water Resour. Res.* 48 (2), W02522. doi:10.1029/2011wr011000

Li, G., Gong, Z., Jiang, W., Zhan, J., Wang, B., Fu, X., et al. (2023). Environmental transport of gyrotactic microorganisms in an open-channel flow. *Water Resour. Res.* 59, e2022WR033229. doi:10.1029/2022WR033229

Li, Y., Xie, L., and Su, T. C. (2020). Profile of suspended sediment concentration in submerged vegetated shallow water flow. *Water Resour. Res.* 56 (4), e2019WR025551. doi:10.1029/2019wr025551

Lu, J., and Dai, H. C. (2016). Large eddy simulation of flow and mass exchange in an embayment with or without vegetation. *Appl. Math. Model.* 40 (17-18), 7751–7767. doi:10.1016/j.apm.2016.03.026

Luhar, M., Rominger, J., and Nepf, H. M. (2008). Interaction between flow, transport and vegetation spatial structure. *Environ. Fluid Mech.* 8, 423–439. doi:10.1007/s10652-008-9080-9

Nepf, H. M. (2012). Flow and transport in regions with aquatic vegetation. *Annu. Rev. Fluid Mech.* 44, 123–142. doi:10.1146/annurev-fluid-120710-101048

Nepf, H. M., and Ghisalberti, M. (2008). Flow and transport in channels with submerged vegetation. *Acta Geophys.* 56 (3), 753–777. doi:10.2478/s11600-008-0017-y

Nepf, H. M., and Vivoni, E. R. (2000). Flow structure in depth-limited, vegetated flow. *J. Geophys. Res.* 105 (C12), 28547–28557. doi:10.1029/2000jc900145

Nezu, I., and Sanjou, M. (2008). Turburence structure and coherent motion in vegetated canopy open-channel flows. *J. Hydro-environment Res.* 2, 62–90. doi:10.1016/j.jher.2008.05.003

Nikora, N., Nikora, V., and O'Donoghue, T. (2013). Velocity profiles in vegetated open-channel flows: Combined effects of multiple mechanisms. *J. Hydraulic Eng.* 139, 1021–1032. doi:10.1061/(asce)hy.1943-7900.0000779

Poggi, D., Krug, C., and Katul, G. G. (2009). Hydraulic resistance of submerged rigid vegetation derived from first-order closure models. *Water Resour. Res.* 45, W10442. doi:10.1029/2008wr007373

Poggi, D., Porporato, A., Ridolfi, L., Albertson, J. D., and Katul, G. G. (2004). The effect of vegetation density on canopy sub-layer turbulence. *Boundary-Layer Meteorol.* 111, 565–587. doi:10.1023/b:boun.0000016576.05621.73

Pourshahbaz, H., Abbasi, S., Pandey, M., Pu, J. H., Taghvaei, P., and Tofangdar, N. (2022). Morphology and hydrodynamics numerical simulation around groynes. *ISH J. Hydraulic Eng.* 28 (1), 53–61. doi:10.1080/09715010.2020.1830000

Pu, J. H., Pandey, M., and Hanmaiahgari, P. R. (2020). Analytical modelling of sidewall turbulence effect on streamwise velocity profile using 2D approach: A comparison of rectangular and trapezoidal open channel flows. *J. Hydro-Environment Res.* 32, 17–25. doi:10.1016/j.jher.2020.06.002

Rominger, J. T., Lightbody, A. F., and Nepf, H. M. (2010). Effects of added vegetation on sand bar stability and stream hydrodynamics. *J. Hydraulic Eng.* 136 (12), 994–1002. doi:10.1061/(asce)hy.1943-7900.0000215

Shan, Y. Q., Zhao, T., and Liu, C. (2020). Turbulence and bed-load transport in channels with randomly distributed emergent patches of model vegetation. *Geophys. Res. Lett.* 47 (12), e2020GL087055.

Shi, J. Z., Li, Y. H., Hughes, J. M. R., and Zhao, M. (2013). Hydrological characteristics of vegetated river flows: A laboratory flume study. *Hydrological Sci. J.* 58 (5), 1047–1058. doi:10.1080/02626667.2013.797580

Shucksmith, J. D., Boxall, J. B., and Guymer, I. (2010). Effects of emergent and submerged natural vegetation on longitudinal mixing in open channel flow. *Water Resour. Res.* 46 (4), W04504. doi:10.1029/2008wr007657

Stoesser, T., Salvador, G. P., Rodi, W., and Diplas, P. (2009). Large eddy simulation of turbulent flow through submerged vegetation. *Transp. Porous Media* 78 (3), 347–365. doi:10.1007/s11242-009-9371-8

Tinoco, R. O. (2020). Simplification bias: Lessons from laboratory and field experiments on flow through aquatic vegetation. *Earth Surf. Process. Landforms* 45 (1), 121–143. doi:10.1002/esp.4743

Tschisgale, S., Löhrer, B., Meller, R., and Fröhlich, J. (2021). Large eddy simulation of the fluid-structure interaction in an abstracted aquatic canopy consisting of flexible blades. *J. Fluid Mech.* 916 (A43), A43–A37. doi:10.1017/jfm.2020.858

Wang, W. J., Huai, W. X., Li, S. L., Wang, P., Wang, Y. F., and Zhang, J. (2019). Analytical solutions of velocity profile in flow through submerged vegetation with variable frontal width. *J. Hydrology* 578, 124088. doi:10.1016/j.jhydrol.2019.124088

Wang, W. J., Peng, W. Q., Huai, W. X., Katul, G., Liu, X. B., Dong, F., et al. (2018). Derivation of canopy resistance in turbulent flow from first- order closure models. *Water* 10, 1782. doi:10.3390/w10121782

Wilson, C. A. M. E., Stoesser, T., Bates, P. D., and Pinzen, A. B. (2003). Open channel flow through different forms of submerged flexible vegetation. *J. Hydraulic Eng.* 129, 847–853. doi:10.1061/(asce)0733-9429(2003)129:11(847)

Wu, H. L., Cheng, N. S., and Chiew, Y. M. (2021a). Bed-load transport in vegetated flows: Phenomena, parametrization, and prediction. *Water Resour. Res.* 57 (4), e2020WR028143. doi:10.1029/2020wr028143

Wu, H. L., Singh, A., Foufoula-Georgiou, E., Guala, M., Fu, X., and Wang, G. (2021b). A velocity-variation-based formulation for bedload particle hops in rivers. *J. Fluid Mech.* 912, A33. doi:10.1017/jfm.2020.1126

Yan, C., Nepf, H. M., Huang, W. X., and Cui, G. X. (2017). Large eddy simulation of flow and scalar transport in a vegetated channel. *Environ. Fluid Mech.* 17 (3), 497–519. doi:10.1007/s10652-016-9503-y

Zeng, C., and Li, C. W. (2014). Measurements and modeling of open-channel flows with finite semi-rigid vegetation patches. *Environ. Fluid Mech.* 14 (1), 113–134. doi:10.1007/s10652-013-9298-z

Zhang, J., Wang, W. J., Shi, H. R., Li, Z., Tang, X., and Xia, Z. H. (2021). An analytical two-layer model for velocity distribution in open-channel flows with submerged flexible canopies considering multiply fluids mechanics. *J. Hydrology* 603, 127102. doi:10.1016/j.jhydrol.2021.127102

Zhao, H. Q., Tang, H. W., Yan, J., Dai, H. C., and Liu, Z. W. (2021). Interactions between bedforms and open channel flows through submerged vegetation. *Adv. Water Sci.* 32 (2), 250–258. (In Chinese).

Zhao, H. Q., Tang, H. W., Yan, J., Liang, D. F., and Zheng, J. Y. (2020). Spectral shortcut in turbulence energy transfer in open channel flow over submerged vegetation. *J. Hydro-environment Res.* 33, 10–18. doi:10.1016/j.jher.2020.10.002

Zhao, H. Q., Yan, J., Yuan, S. Y., Liu, J. F., and Zheng, J. Y. (2019). Effects of submerged vegetation density on turbulent flow characteristics in an open channel. *Water* 11, 2154. doi:10.3390/w11102154

Zhao, T., and Nepf, H. (2021). Turbulence dictates bedload transport in vegetated channels without dependence on stem diameter and arrangement. *Geophys. Res. Lett.* 48, e2021GL095316. doi:10.1029/2021gl095316

Nomenclature

a	the total frontal vegetation area per unit volume
C_d	the drag force coefficient
D	water retention width
d	the zero-plane
F_d	the vegetation resistance term
f	the vortex frequency
K_m	the vortex viscosity coefficient
κ	the von Kármán constant
L	the characteristic length of the vortex size
L_e	characteristic length scale of the mixing layer
l_{eff}	the effective mixing-length scale
N	the total number of samples
S_t	the dimensionless Strouhal number
U	the characteristic flow velocity
U_i	velocity at the inflection point zi
U_{karman}	flow velocity in the Kármán vortex street zone
U_{LL}	the time-averaged velocity
u(t)	the instantaneous velocity in the direction corresponding to the data
u_*	the frictional flow velocity
ν	the kinematic viscosity of water
z_0	the hydrodynamic roughness length
z	the vertical distance calculated from the bottom of the riverbed
δ	Shear layer thickness